Holographic MIMO Surfaces: A Channel Model Approximation in the Electromagnetic Domain

Giovanni Iacovelli, *Member, IEEE,* Claudio Iacovelli, and Symeon Chatzinotas, *Fellow, IEEE*

***Abstract*—This work investigates a Holographic Multiple-Input Multiple-Output (HMIMO) communication system consisting of a source and a receiver being two surfaces in the LoS configuration. The closed-form expressions of the electric field and the channel coupling coefficients are obtained leveraging an asymptotic expansion of the Green's function. The derived approximations show satisfactory accuracy in both near- and far-field conditions, across low and high frequencies. These are then employed to obtain insights regarding (i) the spatial distribution of the beams, and (ii) the mapping relation between source and receiver modes while ensuring sufficient orthogonality under prescribed conditions.**

***Index Terms*—Holographic MIMO, electromagnetic channel, degrees of freedom.**

I. Introduction

HOLOGRAPHIC Multiple-Input Multiple-Output (MIMO) surfaces [1] represent the ultimate evolution of classical MIMO transceivers. The latter are arrays of tiny antennas placed at half-wavelength distance from each other. Each antenna element is equipped with one Radio Frequency (RF) chain, which modulates the signal output for beamforming purposes. Therefore, the antenna positions correspond to the Degrees of Freedom (DoF) of the system, which are thus spatially localized. A Holographic MIMO (HMIMO) surface, instead, virtually embodies an infinite number of low-cost sub-wavelength radiative elements capable to modulate the amplitude of the signal [2]. These surfaces can be equipped with a single RF chain per spatial beam. Collectively, they represent the system DoF, which are spatially delocalized over the whole surface. Unlike classic MIMO, HMIMO continuous nature increases the surface area used for transmitting and receiving signals without requiring a proportional increase in physical size. Henceforth, this novel and simplified design leads to a significant reduction in size, weight, power consumption, and most importantly, cost. Nonetheless, research on this topic is still in its infancy, with recent efforts focusing on fundamental communication aspects, the most relevant being channel modeling [3], [4], beamforming [2] and ergodic capacity [4], [5]. In this context, and according to the specifics of the architecture, HMIMO surfaces are usually mathematically described either as discrete planar arrays or as spatially continuous apertures. In the former case, the infinitesimal element spacing leads to mutual couplings [6], which can be leveraged to achieve super-directivity [7], [8] and hence narrow spatial beams without side-lobes. However, the discrete domain introduces a huge computational complexity in HMIMO signal processing due to the number of radiating units.

In ideal continuous surfaces, instead, mutual couplings are negligible due to the smooth current distribution and the complexity is reduced since there are no discrete elements. Therefore, continuous apertures represent an efficient way to analyze the ultimate performance of HMIMO communication systems. To reach this goal, electromagnetic theory becomes a necessary tool that not only simplifies the derivation of closed-form expressions, but also better aligns with physical reality. In this regard, few works [3], [4] focused on a continuous analysis. A significant contribution is given by [4], where it is considered a scenario in which two holographic segments communicate in Line of Sight (LoS) condition. This configuration is of significant importance to model both high-frequency and long-range communications, where the Non-Line-of-Sight (NLoS) components can be reasonably neglected. In these works, electromagnetic theory and Fourier analysis are employed to derive tractable integral expressions of the electric field and channel model. These results are then leveraged to assess the performance under different signal processing schemes. To the best of the authors' knowledge, the closed-form expressions for the electric field and channel coupling coefficients have not yet been derived. In fact, a more complete and insightful analysis can be carried out with such formulae.

Contribution: In light of the above, in this work it is investigated a scenario in which two continuous HMIMO surfaces of arbitrary size communicate in an unbounded homogeneous mean in a LoS configuration. Starting from electromagnetic theory, the closed-form expressions of the electric field and channel coupling coefficients are obtained by leveraging an asymptotic expansion. The derived approximations show satisfactory accuracy in both near- and far-field conditions, across low- and high frequencies. The consequent analysis provides useful information on the spatial distribution of the beams and their relationship with the electric field. Given a lower-bound on the receiver aperture size, it is demonstrated how source modes map to receiver modes, while ensuring satisfactory orthogonality among DoF. Despite the simplification introduced by the LoS condition, the investigated scenario represents a relevant configuration at the basis of many uses-cases. Indeed, this work is intended to lay the foundation for further development in HMIMO communications between two continuous surfaces by providing analytical insights for a deeper understanding of such systems.

G. Iacovelli and S. Chatzinotas are with the Signal Processing and Communications (SIGCOM) Research Group at Interdisciplinary Centre for Security, Reliability and Trust (SnT), University of Luxembourg, 1855 Luxembourg City, Luxembourg (emails: giovanni.iacovelli@uni.lu, symeon.chatzinotas@uni.lu). C. Iacovelli is an independent researcher (email: claudio.iacovelli@hotmail.it).

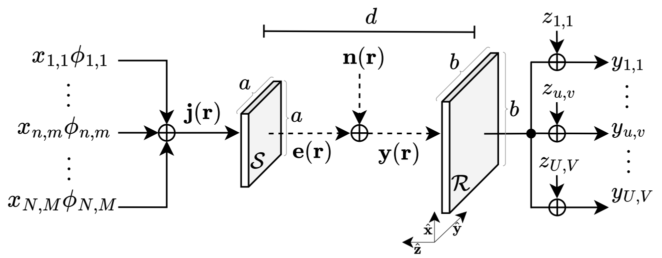

Fig. 1. Transmission scheme between two Holographic MIMO surfaces. The source $\mathcal{S}$ and the receiver $\mathcal{R}$ are centered along $\hat{\mathbf{z}}$, at a distance d, having edges of length a and b, respectively.

II. Electromagnetic Communication Model

The present time-invariant narrowband communication scenario, schematically depicted in Fig. 1, considers two HMIMO surfaces facing each other, namely source $\mathcal{S}$ and receiver $\mathcal{R}$, communicating through an infinite and homogeneous medium, with $\mathbf{r} = [r_x, r_y, r_z]^\mathsf{T} \in \mathbb{R}^3$ being a generic point in the space.

A. Propagation

A monochromatic current density $\mathbf{j}(\mathbf{r}) \in \mathbb{C}^3$, i.e., characterized by a single wavelength λ, at an arbitrary point on the source can be decomposed through a 2D orthonormal basis $\mathbf{\Phi} = \{\boldsymbol{\phi}_{1,1}, \ldots, \boldsymbol{\phi}_{n,m}, \ldots, \boldsymbol{\phi}_{N,M}\}$ with support in $\mathcal{S}$. A maximum of NM symbols $\mathbf{x} = [x_{1,1}, \ldots, x_{n,m}, \ldots, x_{N,M}]^\mathsf{T} \in \mathbb{C}^{NM}$, each one measured in [A], are encoded as

$$\mathbf{j}(\mathbf{r}) = \sum_{m=1}^{M}\sum_{n=1}^{N} x_{n,m}\boldsymbol{\phi}_{n,m}, \tag{1}$$

provided that

$$x_{n,m} = \int_{\mathcal{S}} \boldsymbol{\phi}_{n,m}^\mathsf{H}\, \mathbf{j}(\mathbf{s})\mathrm{d}\mathbf{s}, \quad \int_{\mathcal{S}} \|\mathbf{j}(\mathbf{s})\|^2 \,\mathrm{d}\mathbf{s} \leq p. \tag{2}$$

The latter guarantees that the current density measured in [A/m^2] is square-integrable in $\mathcal{S}$ and has a maximum power p measured in [A^2]. For instance, in waveguide-based architectures [2], this current is generated starting from a baseband signal which carries the information symbols and gets upconverted through RF chains. Each one produces a high-frequency current to excite a feed structure, which then injects an electromagnetic wave into a leaky waveguide. The latter conveys the reference wave to the radiative surface, which finally modulates its amplitude[1] and shapes it into $x_{n,m}\boldsymbol{\phi}_{n,m}$. Consequently, the current signal propagates in free space in the form of an electric field $\mathbf{e}(\mathbf{r}) \in \mathbb{C}^3$, measured in [V/m]:

$$\mathbf{e}(\mathbf{r}) = j\kappa Z_0 \int_{\mathcal{S}} \mathbf{G}(\mathbf{r},\mathbf{s})\mathbf{j}(\mathbf{s})\mathrm{d}\mathbf{s}, \tag{3}$$

where $\kappa = \frac{2\pi}{\lambda}$ denotes the wavenumber, Z_0 represents the characteristic impedance in the vacuum, and

$$\mathbf{G}(\mathbf{r},\mathbf{s}) = \left(\mathbf{I}_3 + \frac{\nabla_\mathbf{r}\nabla_\mathbf{r}^\mathsf{T}}{\kappa^2}\right)\frac{e^{j\kappa\|\mathbf{r}-\mathbf{s}\|}}{4\pi\|\mathbf{r}-\mathbf{s}\|} \in \mathbb{C}^{3\times 3} \tag{4}$$

is the dyadic Green's function.

[1]The outgoing mode $\boldsymbol{\phi}_{n,m}$ can assume an arbitrary shape if the phase of the reference wave can be modulated.

B. Received signal

The field impinging on the receiver surface $\mathcal{R}$ is the sum of the electric field $\mathbf{e}(\mathbf{r})$ generated by the source $\mathcal{S}$ and the electromagnetic noise $\mathbf{n}(\mathbf{r})$ produced by other sources. This is assumed to be an infinite set of planar waves generated in the far-field and received uniformly from all directions. Thus, it can be modeled as a zero-mean complex Gaussian vector $\mathbf{n}(\mathbf{r}) \sim \mathcal{N}_\mathbb{C}(\mathbf{0}_3, \mathbf{C})$ [4]. At the receiver, the incident electromagnetic waves induce a current on the surface, which is then coupled into a waveguide or feed structure. These signals are amplified, downconverted by the RF chains, which introduce a thermal noise $z_{u,v} \sim \mathcal{N}_\mathbb{C}(0, \sigma^2)$, and processed to recover the transmitted data. The coupling between the resulting electric field and waveguides corresponds to a projection on a vector space defined by an orthonormal basis $\Psi = \{\boldsymbol{\psi}_{1,1}, \ldots, \boldsymbol{\psi}_{u,v}, \ldots, \boldsymbol{\psi}_{U,V}\}$ with support in $\mathcal{R}$, so that the scalar form of the received signal samples reads

$$\begin{aligned} y_{u,v} &= \int_{\mathcal{R}} \boldsymbol{\psi}_{u,v}^\mathsf{H}\mathbf{e}(\mathbf{r})\mathrm{d}\mathbf{r} + \underbrace{\int_{\mathcal{R}} \boldsymbol{\psi}_{u,v}^\mathsf{H}\mathbf{n}(\mathbf{r})\mathrm{d}\mathbf{r} + z_{u,v}}_{\eta_{u,v}} \\ &= \sum_{m=1}^{M}\sum_{n=1}^{N} x_{n,m}\underbrace{j\kappa Z_0 \int_{\mathcal{R}}\int_{\mathcal{S}} \boldsymbol{\psi}_{u,v}^\mathsf{H}\mathbf{G}(\mathbf{r},\mathbf{s})\boldsymbol{\phi}_{n,m}\mathrm{d}\mathbf{s}\mathrm{d}\mathbf{r}}_{h_{nm,uv}} + \eta_{u,v} \\ &= \sum_{m=1}^{M}\sum_{n=1}^{N} h_{nm,uv}x_{n,m} + \eta_{u,v}, \end{aligned} \tag{5}$$

where $h_{nm,uv}$ denotes the channel coupling coefficient, as a complex impendence measured in [Ω], between the source and receiver modes. It is possible to recast (5) with $\mathbf{h}_{u,v} = [h_{11,uv}, \ldots, h_{nm,uv}, \ldots, h_{NM,uv}]^\mathsf{T}$ as

$$y_{u,v} = \mathbf{h}_{u,v}^\mathsf{T}\mathbf{x} + \eta_{u,v}, \tag{6}$$

which is the scalar input-output relation of the communication system. To derive fundamental insights about the reference scenario, the following mathematical analysis will focus on the noiseless system without any pre- and/or post-processing. These aspects will be discussed in future works.

III. Proposed Channel Model

In this section, an approximation of the channel model is derived, which is accurate in the near- and far-field.

A. System geometry

The source $\mathcal{S}$ and the receiver $\mathcal{R}$ are regular quadrilaters living in the $\hat{\mathbf{x}}$-$\hat{\mathbf{y}}$-plane with edges of length a and b, respectively. Moreover, they are both centered on and aligned along $\hat{\mathbf{z}}$, facing each other, with $\mathcal{S}$ located at a distance d from the origin, where $\mathcal{R}$ lies. Therefore, the two surfaces domains can be expressed as

$$\mathcal{S} = \{\mathbf{r} \in \mathbb{R}^3 | (r_x, r_y) \in [-\frac{a}{2}, +\frac{a}{2}]\times[-\frac{a}{2}, +\frac{a}{2}], r_z = d\}, \tag{7}$$

$$\mathcal{R} = \{\mathbf{r} \in \mathbb{R}^3 | (r_x, r_y) \in [-\frac{b}{2}, +\frac{b}{2}]\times[-\frac{b}{2}, +\frac{b}{2}], r_z = 0\}. \tag{8}$$

B. Electric Field

First, it is assumed that both the source and the receiver adopt Fourier modes as orthonormal basis. Specifically, the source basis vectors can be expressed[2,3] as

$$\boldsymbol{\phi}_{n,m} = \begin{cases} \frac{1}{\sqrt{2}a} e^{j\frac{2\pi}{a}(\hat{n}r_x + \hat{m}r_y)} \delta(r_z - d)(\hat{\mathbf{x}} + \hat{\mathbf{y}}), & \mathbf{r} \in \mathcal{S} \\ 0, & \mathbf{r} \notin \mathcal{S} \end{cases} \quad (9)$$

with $\hat{n} = -(N-1)/2 + n - 1$, $\hat{m} = -(M-1)/2 + m - 1$, and $N = M = \lfloor 2a/\lambda \rfloor$ being odd integers. The latter can be obtained recalling that the higher spatial frequency is $1/\lambda$. The Dirac delta allows to cast the density coherently with the planar domain (7). Please note that, due to the finite source size, the Fourier transform of the basis is a sinc, which makes its (spatial) spectrum theoretically infinite.

In order to get a definite expression of the electric field, it is necessary to address the integral in (3), but this has not a closed form. First, it is decomposed as $\mathbf{e}(\mathbf{r}) = \sum_{n,m} x_{n,m} \mathbf{e}_{n,m}(\mathbf{r})$, where $\mathbf{e}_{n,m}$ is the electric field of a single source mode (n,m) in (9). Then, it is assumed that $d - r_z \equiv q_z$ becomes the dominant length scale of the system $q_z \gg \max(a,b)$, such that a Taylor expansion in $q_z \to \infty$ of $\mathbf{e}_{n,m}$ can be truncated at the first order. It is worth specifying that this approach does not necessarily impose a far-field condition, which instead is defined for $q_z \geq 2\max(a,b)^2\lambda^{-1}$. Recalling that (i) $\mathbf{G}(\mathbf{r},\mathbf{s})$ in (4) is the only function dependent on q_z when the Dirac delta in (9) simplifies the s_z-integration in (3); (ii) the whole integrand in (3), for a sufficiently large q_z, is absolutely integrable, i.e., absence of divergence in the integration domain; then, it is possible to pass the series operator into the integral and expand only the propagator. Hence, the integral which corresponds to the approximated expression of the single-mode electric field reads

$$\mathbf{e}_{n,m}(\mathbf{r}) \simeq \frac{jZ_0(\hat{\mathbf{x}} + \hat{\mathbf{y}})}{2\sqrt{2}\lambda q_z a} \iint_{[-\frac{a}{2},+\frac{a}{2}]\times[-\frac{a}{2},+\frac{a}{2}]} e^{j2\pi\left(\frac{\hat{n}s_x + \hat{m}s_y}{a} + \frac{\Delta_x^2 + \Delta_y^2 + 2q_z^2}{2\lambda q_z}\right)} \mathrm{d}s_x \mathrm{d}s_y,$$

with $\Delta_x = r_x - s_x$, $\Delta_y = r_y - s_y$. Observe that the integrand is at most quadratic in the exponent with respect to the integration coordinates and also factorized in the two directions. By completing the squares, the integrand is rewritten as a product of two complex Gaussians, whose primitive is the complex error function $\mathrm{Erfi}(x)$. The closed-form expression of the single-mode electric field reads

$$\mathbf{e}_{n,m}(\mathbf{r}) = \frac{Z_0(\hat{\mathbf{x}} + \hat{\mathbf{y}})}{8\sqrt{2}a} e^{\frac{j\pi 2q_z}{\lambda}} \mathcal{E}(r_x, \hat{n}) \mathcal{E}(r_y, \hat{m}), \quad (10)$$

$$\mathcal{E}(r, \hat{i}) = e^{\frac{j\pi}{a^2}(2a\hat{i}r - q_z\lambda\hat{i}^2)} \sum_{l=0}^{1} \mathrm{Erfi}\left(\alpha_1(a + (-1)^l 2(r - \alpha_2\hat{i}))\right).$$

Here, $\alpha_1 = \sqrt{j\pi}/(2\sqrt{q_z\lambda})$, $\alpha_2 = q_z\lambda/a$, $r \in \{r_x, r_y\}$ and $\hat{i} \in \{\hat{n}, \hat{m}\}$. The null $\hat{\mathbf{z}}$ component arises from the geometry of the scenario, which produces only $\mathcal{O}(q_z^{-2})$ terms in the Taylor series, but these are neglected due to the applied truncation.

C. Channel coupling coefficients

Similarly to the source case, it is assumed that also the receiver adopts Fourier modes as orthonormal basis

$$\boldsymbol{\psi}_{u,v} = \begin{cases} \frac{1}{\sqrt{2}b} e^{j\frac{2\pi}{b}(\hat{u}r_x + \hat{v}r_y)} \delta(r_z)(\hat{\mathbf{x}} + \hat{\mathbf{y}}), & \mathbf{r} \in \mathcal{R} \\ 0, & \mathbf{r} \notin \mathcal{R} \end{cases} \quad (11)$$

with obvious definitions of $\hat{u}, \hat{v} \in [-b/\lambda, b/\lambda]$. Note that the spatial frequencies are proportional to the receiver size, which is generally different from the source one, so that $U = V = \lfloor 2b/\lambda \rfloor$. Also, the Dirac delta centers the basis set in the origin in accordance with the domain (8).

The channel coupling coefficients in (5) can be expressed as a definite integral through the evaluation of the primitive $h^{\mathsf{P}}_{nm,uv}(r_x, r_y) = \iint \boldsymbol{\psi}^{\mathsf{H}}_{u,v} \mathbf{e}_{n,m}(\mathbf{r}) \mathrm{d}\mathbf{r}$ in the receiver vertices

$$\begin{aligned} h_{nm,uv} &= h^{\mathsf{P}}_{nm,uv}(-b/2, -b/2) + h^{\mathsf{P}}_{nm,uv}(b/2, b/2) \\ &\quad - h^{\mathsf{P}}_{nm,uv}(b/2, -b/2) - h^{\mathsf{P}}_{nm,uv}(b/2, -b/2), \end{aligned} \quad (12)$$

where the closed-form expression of the primitive is

$$h^{\mathsf{P}}_{nm,uv}(r_x, r_y) \simeq -\frac{Z_0 ab e^{-\frac{2j\pi d}{\lambda}}}{8\pi^3} \mathcal{H}(r_x, \hat{n}, \hat{u}) \mathcal{H}(r_y, \hat{m}, \hat{v}),$$

$$\mathcal{H}(r, \hat{i}, \hat{l}) = \frac{e^{-j\pi\left(\frac{2\hat{i}r}{b} + \hat{i} - \frac{(a+2r)^2}{4d\lambda}\right)}}{a\hat{l} - b\hat{i}} \left(\Delta^+_{\mathcal{D}} + e^{2j\pi\left(\hat{i} - \frac{r}{\alpha_2}\right)} \Delta^-_{\mathcal{D}}\right),$$

$$\Delta^+_{\mathcal{D}}(r, \hat{i}, \hat{l}) = \mathcal{D}\big(\beta_1(a + 2(r - \beta_2\hat{l}))\big) - \mathcal{D}\big(\beta_1(a + 2(r - \alpha_2\hat{i}))\big),$$

$$\Delta^-_{\mathcal{D}}(r, \hat{i}, \hat{l}) = \mathcal{D}\big(\beta_1(a - 2(r - \beta_2\hat{l}))\big) - \mathcal{D}\big(\beta_1(a - 2(r - \alpha_2\hat{i}))\big).$$

For compactness, the arguments of $\Delta^{\pm}_{\mathcal{D}}$ in $\mathcal{H}(r, \hat{i}, \hat{l})$ have been suppressed. Further, $\beta_1 = (1+j)\sqrt{\pi}/(2\sqrt{2d\lambda})$, $\beta_2 = d\lambda/b$, $\hat{l} \in \{\hat{u}, \hat{v}\}$ and $\mathcal{D}(x) = \sqrt{\pi}/2 e^{-x^2} \mathrm{Erfi}(x)$ is the Dawson function.

To validate the accuracy of the proposed model, Fig. 2 compares the real and imaginary parts of the exact solution and the closed-form approximation of $h_{nm,uv}$ for $\hat{n} = \hat{m} = \hat{u} = \hat{v} = 0$ derived in (5) and (12), respectively. The model provides a remarkable accuracy, not only in far-field but also in a region of near-field which depends on the wavelength. Indeed, there is a discrepancy between the exact and approximated curves for $\lambda = 0.01$ before the 5 meter range. This is due to the higher order contributions, i.e $O(q_z^{-2})$, which are neglected in the truncated Taylor expansion employed for the single-mode electric field (10), in turn involved in (12).

Relevantly, if the surfaces are electromagnetically large, i.e. $a/\lambda, b/\lambda \gg 1$, then any slowly varying function can be well approximated by a discrete Fourier series of the modes considered in this work. Therefore, the coupling channel coefficients between arbitrary bases $\boldsymbol{\Phi}$ and $\boldsymbol{\Psi}$ can be expressed as linear combinations of (12).

With this in mind, and for the considered LoS scenario, these couplings can be readily computed to predict signals strengths (5), which are employed in current experimental schemes for the outdoor validation of HMIMO prototypes [9].

[2]If the waveguide modes are also assumed to be plane waves, no phase nor amplitude modulation is needed to achieve this basis set. Indeed, it is sufficient to adjust the feed positions to suppress the interference [2].

[3]The Dirac delta is not a square integrable function, therefore (2) diverges when plugging (9). This conflict is lifted by mere replacement $\delta^2(.) \to \delta(.)$, conveniently understood with a quantum mechanical bra-ket notation, where deltas are the representation in position-r_z space of the position eigenstate $|d\rangle$, i.e. $\delta(r_z - d) \equiv \langle r_z|d\rangle$. Since kets $|.\rangle$ must be normalized to unity, i.e. $\langle .|.\rangle = 1$, and the completeness relation of the basis reads $\int \mathrm{d}r_z |r_z\rangle\langle r_z| = \mathbb{I}$, the divergence is solved as $\int \mathrm{d}r_z \delta^2(r_z - d) = \int \mathrm{d}r_z \langle d|r_z\rangle\langle r_z|d\rangle = \langle d|d\rangle = 1$.

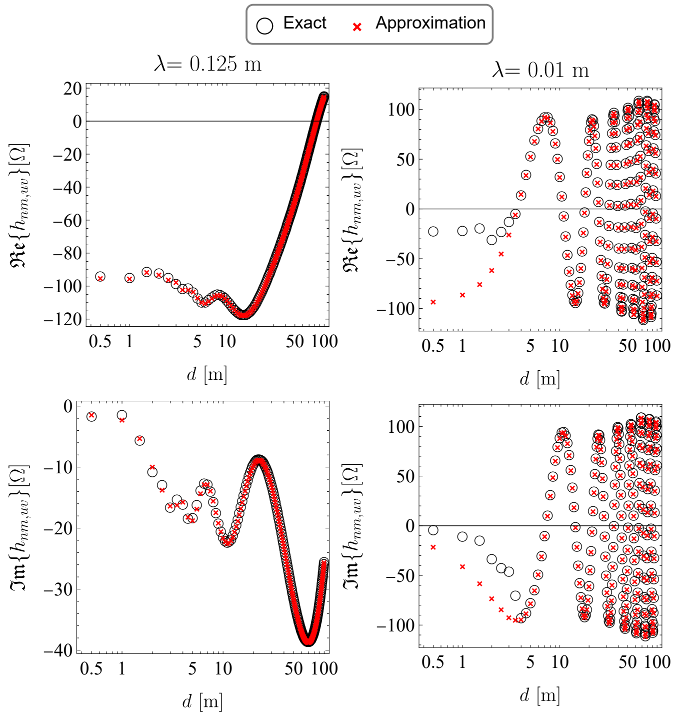

Fig. 2. Comparison between exact and approximated channel for $a = 1$ m, $b = 2$ m, and $\hat{n} = \hat{m} = \hat{u} = \hat{v} = 0$.

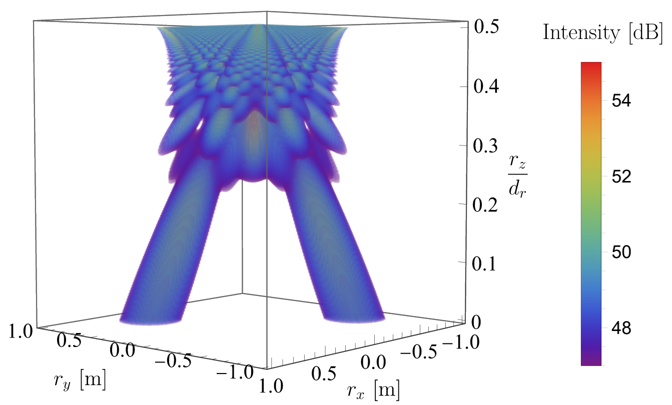

Fig. 3. Electric field intensity generated by two source modes $(\hat{n}, \hat{m}) = \{(1, 0), (0, 1)\}$ for $a = 1$ m, $d = 50$ m, $\lambda = 0.01$ m.

IV. Analytical Results

In this Section, the above derivations are employed to obtain analytical results useful to grasp the advantages and limitations of the investigated HMIMO communication system.

A. Degrees of Freedom and Spatial Beams

The number of DoF $NM = \lfloor 4a^2/\lambda^2 \rfloor$ at the source, corresponding to the number of orthogonal spatial beams generated, is in practice limited at the receiver side by different factors. Provided that no additional analog and/or digital processing is performed, only a subset of those beams directly impinge on the receiver surface due to their different propagation directions. Specifically, this subset can be derived by requesting that the peak of the beams fall in the receiver surface region. To obtain their coordinates, the gradient of the electric field intensity with respect to r_x, r_y is imposed to zero

$$\nabla_{\mathbf{r}} \|\mathbf{e}_{n,m}(\mathbf{r})\|^2 = \mathbf{0}_2 \Longrightarrow \bar{r}_x = \alpha_2(\hat{n}+c_1), \bar{r}_y = \alpha_2(\hat{m}+c_2), \quad (13)$$

where $c_1, c_2 \in \mathbb{Z}$, and the receiver surface is selected with $r_z = 0$, i.e., $q_z = d$. Note that the maximum is obtained for $c_1, c_2 = 0$ (the center of the wavepacket) already for a distance d smaller than the Rayleigh distance $d_r = a^2/\lambda$. In fact, beyond this region, as shown in Fig. 3, the spatial beams naturally emerge from the source as a consequence of coherent sum in the diffraction phenomenon. Then, the source modes whose peaks (13) fall in the receiver surface, i.e. $\hat{n}, \hat{m} \in [-b\alpha_2/2, +b\alpha_2/2]$, are found by imposing $\bar{r}_x, \bar{r}_y \in [-b/2, +b/2]$. Thus, the total number of DoF available at the receiver is $\left\lfloor \frac{ba}{\lambda d} \right\rfloor^2 + 1$ (paraxial approximation) where the additional one is the zeroth mode seen in far-field.

Finally, the peak coordinates at the receiver, as a function of the elevation angle $\theta_{n,m}$, read:

$$d/\sqrt{\bar{r}_x^2 + \bar{r}_y^2} = \tan\theta_{n,m} \Longrightarrow \theta_{n,m} = \arctan \frac{a}{\lambda\sqrt{\hat{n}^2 + \hat{m}^2}}. \quad (14)$$

B. Channel Coupling Maximization

A map between the source and receiver modes is obtained by maximizing the channel coupling coefficients with respect to the latter. These extremal modes do not admit a simple expression as functions of the source DoF, unless (12) is taken for asymptotically large receiver apertures:

$$\bar{h}_{nm,uv} = \frac{(-1)^{\hat{n}+\hat{m}} \sin\left(\frac{\pi a \hat{u}}{b}\right) \sin\left(\frac{\pi a \hat{v}}{b}\right) e^{\frac{j\pi d}{\lambda}\left(2 - \frac{\lambda^2}{b^2}(\hat{u}^2 + \hat{v}^2)\right)}}{(a\hat{u} - b\hat{n})(a\hat{v} - b\hat{m})} \xi, \quad (15)$$

where $\xi = -abZ_0/(2\pi^2)$. Observe that this expression does not scale with d because an infinite receiver captures half of the whole electric field at any distance. It is deduced by replacing the complex error functions in the Dawsons with their asymptotic behavior $\lim_{b\to\infty} \mathrm{Erfi}((1+j)b) = j$. This approximation holds valid when

$$b \geq 2\max(|\bar{r}_x|, |\bar{r}_y|) + a + 2\varepsilon\sqrt{2\lambda d/\pi}, \quad (16)$$

where $\bar{r}_x$ and $\bar{r}_y$ in (13) are evaluated at $c_1 = c_2 = r_z = 0$ and $\varepsilon \in \mathbb{R}_+$ is a parameter determining how accurate the limit approximation is ($\varepsilon \geq 2$ already provides good results). This condition guarantees that b is sufficiently large to dominate every lengthscale in the arguments of the $\mathrm{Erfi}(x)$ which appear in the channel formula. In this regime, the actual exploitable DoF are computed by squaring (16) set at equality for a fixed b, to retrieve $\max(\hat{n}^2, \hat{m}^2)$. As shown in Fig. 4, this results in fewer DoF compared to the paraxial approximation. Finally, if (16) holds, the receiving modes which maximize the asymptotic couplings (15) can be computed as

$$\nabla_{u,v} |\bar{h}_{nm,uv}|^2 = \mathbf{0}_2 \implies \bar{\hat{u}} = \frac{b}{a}\hat{n}, \bar{\hat{v}} = \frac{b}{a}\hat{m}. \quad (17)$$

This result shows that the receiver mode which maximizes (15) is the source mode rescaled by the ratio between the surfaces' sizes. As a consequence, the receiver aperture b must be a multiple integer of the source a to not spread the signal among adjacent modes.

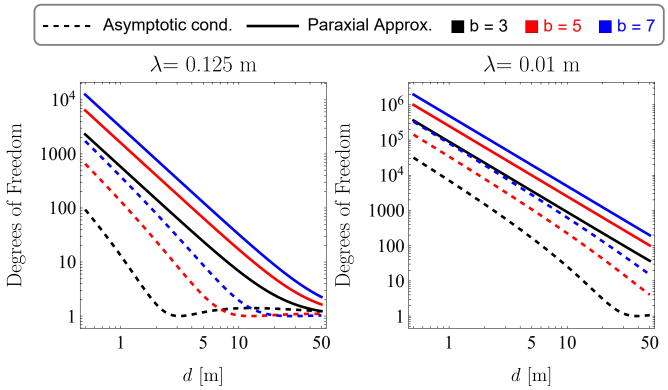

Fig. 4. Number of DoF for $a = 1$ m, $\lambda = 0.01$ m, and $\varepsilon = 2$.

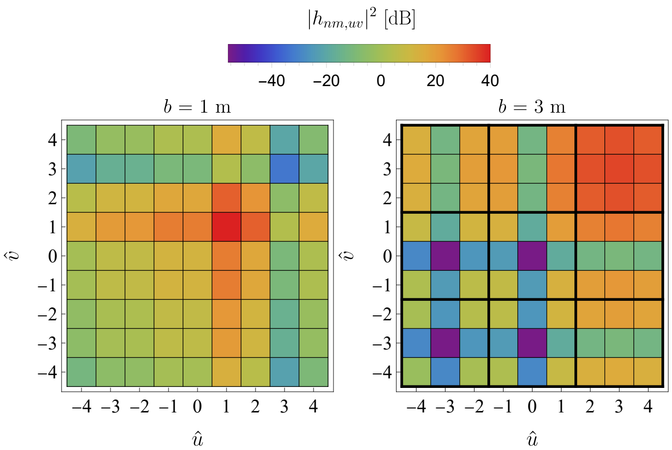

Fig. 5. Crosstalk comparison for $a = 1$ m, $d = 25$ m, $\lambda = 0.01$ m, and $\hat{n} = \hat{m} = 1$. For $b = 1$ m, the adjacent modes receive $\sim$30 dB. Despite a loss of $\sim$5 dB, for $b = 3$ m, the modes at a distance b/a given by (17) receive only -10 dB. Here, (16) is satisfied with $\varepsilon = 2$.

C. Orthogonality Discussion

The presence of the complex error function in (10) and (12) is the result of Green's function integration in a bounded spatial domain. This is similar to the sinc function arising in place of the Dirac delta from the Fourier transform of a constant when the domain is bounded. Therefore, crosstalk among spatial modes is an unavoidable and direct consequence of having a finite receiver surface, but also of electromagnetic theory at the basis of HMIMO communications. In fact, in traditional wireless systems, the channel impulse response is typically finite in time due to the limited delay spread of multipath components. This allows for the use of a cyclic prefix, which converts linear- into circular- convolution, to preserve orthogonality among subcarriers, thus mitigating inter-symbol interference. Instead, in the HMIMO framework, the channel impulse response corresponds to the Green's function (4) and its support extends to spatial infinity. Then, (16) is required to achieve a certain degree of orthogonality, with the last term acting as the cyclic prefix in traditional systems. In this regard, Fig. 5 quantifies the crosstalk among receiver modes depending on whether (16) is satisfied or not.

V. Conclusion and Future Works

In this work, by means of a first-order asymptotic expansion, the closed-form expression of the electric field and the channel coupling coefficients are provided for a LoS HMIMO system.

Significant accuracy is achieved already in the near-field regime for both centimeter and millimeter wavelength communications. A comprehensive analysis is carried out leveraging these expressions. Specifically, the electric field approximation is maximized to obtain the peak locations. These positions lead to the same result of the paraxial approximation when estimating the number of DoF as the number of incident beams. Subsequently, to obtain an I/O relation between source and receiver DoF, the coupling coefficient approximation is maximized with respect to the receiver modes as a function of the source ones, in the limit of a large receiver aperture. This condition allows to achieve a certain degree of orthogonality among receiver modes at the cost of reducing the number of effective DoF. Future research will generalize the channel model by parametrizing the position and tilt of the source with respect to the receiver in three dimensions. In addition, a stochastic model that addresses NLoS configurations can be deduced when treating such parameters as random variables. Moreover, since the channel operator can be treated with the proposed approximation, a current basis derived from its eigenfunctions can give rise to a quasi-optimal scheme. Further, continuous real-valued multi-user beamformers should be designed to assess more practical applications.

The pursuit of these avenues, built on the groundwork laid in this study, will bridge the gap between theoretical findings and practical applications in HMIMO systems.

References

[1] T. Gong, P. Gavriilidis, R. Ji, C. Huang, G. C. Alexandropoulos, L. Wei, Z. Zhang, M. Debbah, H. V. Poor, and C. Yuen, "Holographic MIMO Communications: Theoretical Foundations, Enabling Technologies, and Future Directions," *IEEE Commun. Surv. Tut.*, vol. 26, no. 1, pp. 196–257, 2024.

[2] R. Deng, B. Di, H. Zhang, Y. Tan, and L. Song, "Reconfigurable Holographic Surface-Enabled Multi-User Wireless Communications: Amplitude-Controlled Holographic Beamforming," *IEEE Trans. Wireless Commun.*, vol. 21, no. 8, pp. 6003–6017, 2022.

[3] A. Pizzo, L. Sanguinetti, and T. L. Marzetta, "Fourier Plane-Wave Series Expansion for Holographic MIMO Communications," *IEEE Trans. Wireless Commun.*, vol. 21, no. 9, pp. 6890–6905, 2022.

[4] L. Sanguinetti, A. A. D'Amico, and M. Debbah, "Wavenumber-Division Multiplexing in Line-of-Sight Holographic MIMO Communications," *IEEE Trans. Wireless Commun.*, vol. 22, no. 4, pp. 2186–2201, 2023.

[5] S. Zeng, H. Zhang, B. Di, Z. Han, and H. Vincent Poor, "Dual-Polarized Reconfigurable Intelligent Surface-Based Antenna for Holographic MIMO Communications," *IEEE Trans. Wireless Commun.*, pp. 1–1, 2024.

[6] E. Björnson, L. Sanguinetti, H. Wymeersch, J. Hoydis, and T. L. Marzetta, "Massive MIMO is a reality—What is next?: Five promising research directions for antenna arrays," *Digit. Signal Process.*, vol. 94, pp. 3–20, 2019, special Issue on Source Localization in Massive MIMO.

[7] A. A. D'Amico and L. Sanguinetti, "Holographic MIMO Communications: What is the Benefit of Closely Spaced Antennas?" *IEEE Trans. Wireless Commun.*, pp. 1–1, 2024.

[8] B. Tadele, V. Shyianov, F. Bellili, and A. Mezghani, "Channel Estimation for Multicarrier Systems with Tightly-Coupled Broadband Arrays," 2023. [Online]. Available: https://arxiv.org/abs/2304.07440

[9] Staff, Pivotal, "Holographic Beam Forming Improves Mid-Band Radio Link Performance," *Pivotal Commware, Inc., Kirkland, WA, USA*, 2022. [Online]. Available: https://pivotalcommware.com/wp-content/uploads/2022/05/Mid-Band-White-Paper.pdf